

Institutions of the Russian Academy of Sciences
Joint Institute for High Temperatures RAS
Institute of Problems of Chemical Physics RAS
Kabardino-Balkarian State University

Physics of Extreme States of Matter — 2011

Chernogolovka, 2011

Physics of Extreme States of Matter — 2011

Edited by academician Fortov V. E., Karamurзов B. S., Temrokov A. I., Efremov V. P., Khishchenko K. V., Sultanov V. G., Levashov P. R., Andreev N. E., Kanel G. I., Iosilevskiy I. L., Milyavskiy V. V., Mintsev V. B., Petrov O. F., Savintsev A. P., Shpatakovskaya G. V.

This compendium is devoted to investigations in the fields of physics of high energy densities and thermophysics of extreme states of matter. Interaction of intense laser, x-ray and microwave radiation, powerful particle beams with matter, techniques of intense energy fluxes generation, physics of shock and detonation waves, experimental methods of diagnostics of ultrafast processes, different models and results of theoretical calculations of equations of state of matter at high pressures and temperatures, low-temperature plasma physics, issues of physics and power engineering, as well as technology projects are considered. The majority of the works has been presented at the XXVI International Conference on Interaction of Intense Energy Fluxes with Matter (March 1–6, 2011, Elbrus, Kabardino-Balkaria, Russia). The edition is intended for specialists in physical and technical problems of power engineering.

The conference is sponsored by the Russian Academy of Sciences and the Russian Foundation for Basic Research (grant No. 11-02-06033).

ISBN 978-5-901675-96-0

© Institute of Problems of Chemical Physics, Russian Academy of Sciences,
Chernogolovka, 2011

high dynamical registration range, high apprehensibility which allow to register the soft X-ray emission with $\sim 0.6mkm$ resolution for one laser flash [2]. Diffraction pattern obtained by the detector from each cell (*fig.2*) then was compared with diffraction pattern obtained by means of numerical simulation (*fig.3*). Chosen model parameters for optimal coincidence with experimental data we can restore real beam parameters for each cell.

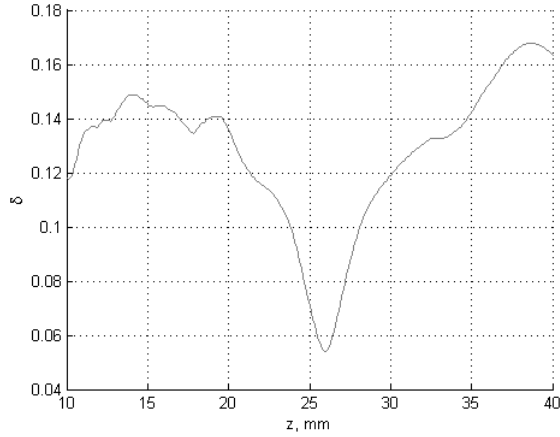


Figure 6. δ value dependence from the distance between mesh and detector

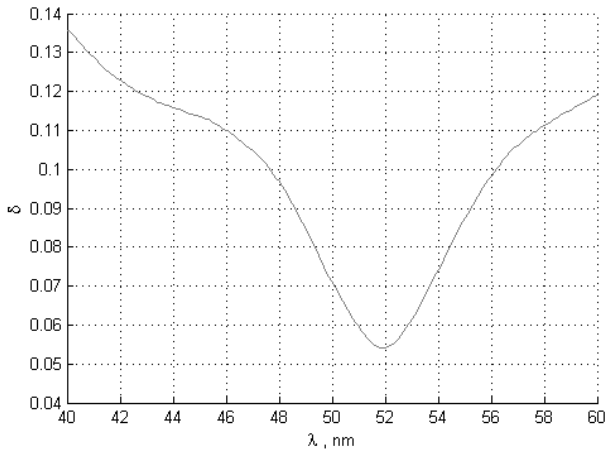


Figure 7. δ value dependence from the wavelength

Experimental X-ray intensity distribution formed by its diffraction on a wire (2 line) and its numerical simulation (1 line) are shown on the *fig.4*. Numerical simulation has been performed using the following set

of parameters: wire thickness $d = 36.5mkm$, distance between mesh and detector $z = 26mm$, wave length $\lambda = 52nm$, coherence distance $L_c = 100mkm$. The value δ which describes the average deviation of calculated distribution from the experimental one on the section $x = [-150, 0]$ was used for comparison of experimental and calculated distributions. For this set of parameter the $\delta = 0.045$.

Parabolic wave equation was used for modeling of beam propagation:

$$2ik \frac{\partial u}{\partial z} + \frac{\partial^2 u}{\partial x^2} + \frac{\partial^2 u}{\partial y^2} = 0 \quad (1)$$

3D field distribution can be found through field distribution on the $z = 0$ plane:

$$u(x, y, z) = \sqrt{\frac{k}{2\pi iz}} \int_{-\infty}^{\infty} u_0(\xi, \eta) e^{ik \frac{(x-\xi)^2 + (y-\eta)^2}{2z}} d\xi d\eta. \quad (2)$$

All the parameters were changed separately to determine the method sensitivity to the change of the parameters. Obtained intensity distribution was compared to the experimental distribution (with parameters unchanged). The \hat{I} value dependence from the wire thickness, the distance between mesh and detector and the wavelength are presented on the Fig. 5, 6, 7, respectively. These figures show that even small (less than 10%) parameters deviation from the optimal values lead to considerable increase of δ .

The method also allows to determine the beam spectral width line. In this case it is $1nm$ and its in a good agreement with the spectral width line obtained from another method.

In this studying experimentally and theoretically was shown what introduced method allow to measure the intensity, coherence and spectral behaviour of soft X-ray laser beam distribution across the beam profile with accuracy better than 10%.

1. Inagaki T., Imoue S., Ishi M. et al. A compact free-electron laser for generating coherent radiation in the extreme ultraviolet region, *Nature Photonics*, 2008, t.2, c. 555
2. Faenov A.Ya., Kato Y., Tanaka M., et al., Submicrometer-resolution in situ imaging of the focus pattern of a soft x-ray laser by color center formation in LiF crystal, *Optics Letters*, 2009, t. 34, c.941

ABLATION OF LITHIUM FLUORIDE DIELECTRIC CRYSTAL BY ULTRASHORT PULSES OF X-RAY PLASMA LASER AND EXTREME ULTRAVIOLET FREE ELECTRON LASER

*Anisimov S.I.*¹, *Faenov A.Ya.*², *Inogamov N.A.*¹, *Khokhlov V.A.*¹, *Petrov Yu.V.*^{*1},
*Skobelev I.Yu.*², *Zhakhovskii V.V.*²

¹*ITP RAS, Chernogolovka,* ²*JIHT RAS, Moscow, Russia*

**uvp49@mail.ru*

We present results of two sets of ablation experiments with the dielectric target on soft X-ray lasers, a physical modeling and computer simulation of these

experiments. Experiments were made at two distinct X-ray lasers, different in pulse duration τ_L and photon energy ε_γ with a wide gap lithium fluoride (LiF)

dielectric as a target.

First of them was carried out at Ag X-ray laser (Ag XRL) of Kansai Photon Science Institute of Japan Atomic Energy Agency. Laser system generates a completely coherent XRL beam with the wave length $\lambda = 13.9$ nm, average pulse energy 300 nJ and pulse duration $\tau_L = 7$ ps. The XRL beam was focused on a LiF crystal of 2 mm thickness and 20 mm diameter by a spherical Mo/Si multilayer mirror. To record the beam patterns at different focusing distances and to fresh a target surface after each shot the LiF crystal was moved along and perpendicular to the propagation direction. After traversing the Zr filter (in order to reduce the scattered optical radiation and the thermal X-ray emission from the plasma produced by ps optical laser) and Mo/Si mirror the total energy of the XRL pulse on the LiF crystal was $\simeq 75$ nJ in each shot.

The second set of experiments with the use of the self-amplified spontaneous-emission free electron laser (SASE-FEL) facility has been conducted at the SPring-8 Compact SASE Source (SCSS). This device can provide laser pulses in the extreme-ultraviolet (EUV) region with wave length 51-62 nm (61.5 nm in our experiments). SCSS pulse energy have been varied from 4 to 11 μJ in different shots, the pulse duration was about 300 fs. The Kirkpatrick-Baez microscope, based on ellipsoidal and cylindrical mirrors coated by SiC multilayers was used to focus EUV beam at the distance about 100 cm from the mirror output. Again the LiF crystal has been shifted along the FEL beam propagation direction and also perpendicular to it after each shot. To find the ablation threshold of LiF crystals, we varied EUV-FEL energy and/or change a focusing position from the best focus at the surface of a LiF crystal to defocusing from the best focus up to 40 mm. The luminescence of stable color centers (CCs), formed by the XRL radiation, was used to measure the laser fluence distribution in the Ag XRL and SCSS laser focal spots. This is very important as it allows us to define the accurate value of the real local fluence at a target surface. This improvement (with marking of the intensity distribution by the CCs) allows to find exact values of the ablation threshold. This is significant since, due to the strong aberrations, the intensity distribution has complicated and smeared-out shape and only a small part (10-30%) of pulse energy is localized within the ablation crater near the ablation threshold. To confirm that the surface of crystal has been damaged, we used an OLYMPUS BX60 microscope. In addition, cross sections of the ablated craters were measured by the atomic force microscope (AFM, TOPOMETRIX Explorer) operating in the tapping mode. Typical images of the Ag XRL and SCSS laser beams, recorded on the LiF crystal at different focusing positions, are presented in Figure 1.

Target surface images in luminescence and visible modes in experiments with Ag XRL are shown in Fig. 1 a. As it is obviously seen from this Figure, our new experimental results exhibited a low value for the ablation threshold $F_{abl} \simeq 10$ mJ/cm². This value is much lower than the ablation thresholds for ns XRL and for fs, ns optical lasers. The SCSS beam allows to

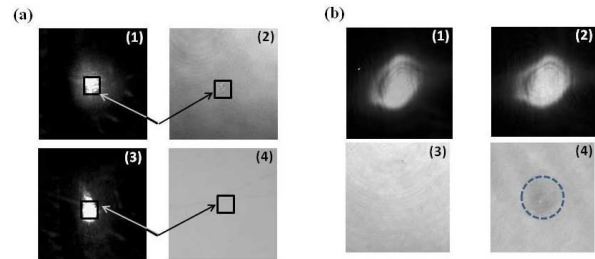


Figure 1. a) The patterns of the Ag XRL irradiation recorded on LiF crystal. The crystal is placed in the best focusing position and 1 mm out of it. b) The patterns irradiated by EUV-FEL and recorded on LiF crystal, placed in the best focusing position and 26 mm out of it. Images were obtained by Olympus microscope working at luminescent and visible modes. The area of ablation is marked on the visible images.

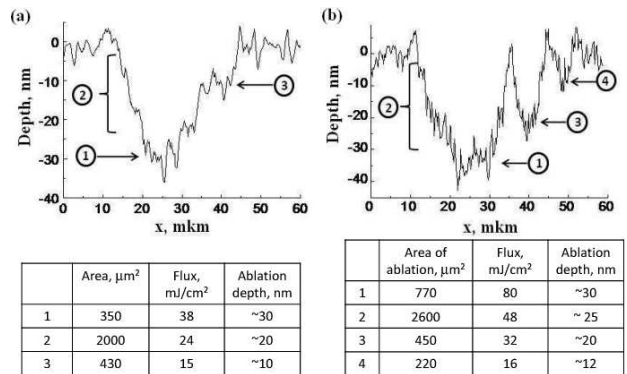


Figure 2. Traces from AFM images of patterns recorded on LiF crystal placed 5 mm apart from the best focusing position (a-for the EUV-FEL beam energy $E=5.3\mu\text{J}$, b-for $E\approx 11\mu\text{J}$). Traces show that different ablation zones could be selected, which correspond to laser fluences from 16 to 80 mJ/cm². These different zones are marked by digits 1, 2, 3 (for pulse energy 5.3 μJ) or 1-4 (10.8 μJ). The corresponding ablated depths for them are listed in Tables. Small change of an ablation depth from $\simeq 12$ nm to $\simeq 30$ nm with significant increasing of laser fluence has been observed.

measure laser beam energy in each shot and to obtain damage on LiF crystal on large areas and in much wider range of laser fluences. This is important advantages of the SCSS device in comparison with the Ag XRL. As it can be seen from Fig. 1 b, damages on the surface of LiF crystals, due to the action of SCSS beam, were observed not only in the case of placing of a LiF crystal in the best focusing position, but also even in the case when crystal was 26 mm out of focus. In the later case, the size of ablation zone had reached a very large value $\simeq 0.35$ mm². Large defocusing of the EUV-FEL beam and irradiation of target by pulses with different EUV-FEL intensities permitted, essentially, to vary laser flux and to measure the LiF ablation threshold accurate enough. From Figure 1 b we can see that fluence $\simeq 7.1$ mJ/cm² is not sufficient yet for EUV-FEL production of ablation on the surface of LiF crystal. Meanwhile, fluence $\simeq 9.2$ mJ/cm² was sufficient to produce clear spot on the surface of the LiF crystal. When comparing the changes of ab-

lation depth in different ablation zones, irradiated by EUV-FEL with different fluencies, we have determined that the smallest depth, which appears near ablation threshold of LiF crystal, is 10-15 nm. Meanwhile, increasing laser fluence up to 80 mJ/cm² does not efficiently increase the ablation depth, which reaches the value of only about 30-35 nm. This result is different enough in comparison with irradiation of LiF crystals by 7 ps Ag XRL laser where we observed the depths of ablation about 40-50 nm near the ablation threshold. Irradiation of LiF crystals at even greater intensities shows the slow increase of ablation depth with increasing of EUV-FEL fluence. Even for fluences of EUV-FEL about 110 -150 mJ/cm² the ablation depth is quite small and varied around 30-40 nm.

When theoretically considering the ablation of LiF under the action of ultrashort XRL pulses we use the system of Lagrangian hydrodynamic equations:

$$n \frac{\partial Z}{\partial t} = \frac{I}{\varepsilon_\gamma D_{att}} + \nu_{imp} n_e - \kappa_r n_e^3 \quad (1)$$

$$\rho_0 \frac{\partial E_e / \rho}{\partial t} = \frac{\rho_0 I}{\rho D_{att}} - n \Delta \frac{\partial Z}{\partial t} - \frac{\rho_0}{\rho} \alpha (T_e - T_i) - p_e \frac{\partial u}{\partial x^0} \quad (2)$$

$$\rho_0 \frac{\partial E_i / \rho}{\partial t} = \frac{\rho_0 I}{\rho D_{att}} - \frac{\rho_0}{\rho} \alpha (T_e - T_i) - p_i \frac{\partial u}{\partial x^0} \quad (3)$$

$$\rho_0 \frac{\partial u}{\partial t} = - \frac{\partial p}{\partial x^0} \quad (4)$$

$$\rho(x^0, t) \frac{\partial x(x^0, t)}{\partial t} = \rho^0 \quad (5)$$

$$\frac{\partial x(x^0, t)}{\partial t} = u(x^0, t) \quad (6)$$

Here E_i , T_i , p_i , and E_e , T_e , p_e are internal energy, temperature and pressure of ions and conduction electrons correspondently, $Z = n_e/n$ is the ionization degree of LiF pairs with the concentration n . ρ is a density with its initial value ρ_0 , Lagrangian variable x^0 is the initial position of material particle. Attenuation depth $D_{att}=9$ nm for the photon energy $\varepsilon_\gamma=20.2$ eV in EUV-FEL is equal to 9 nm. Laser energy flux in (1,2) has a form:

$$I(x^0, t) = \frac{F}{\sqrt{\pi} \tau_L} \exp\left(-\frac{t^2}{\tau_L^2}\right) \exp\left(-\frac{x^0}{D_{att}}\right) \quad (7)$$

Comparison of thermodynamical properties of LIF and aluminum[1] exhibits the similarity of their equations of state (in Fig. 3 cold pressure and Hugoniot adiabatas of these two materials are shown). It allows us to use the equation of state of aluminum to obtain the ionic contribution E_i to the internal energy

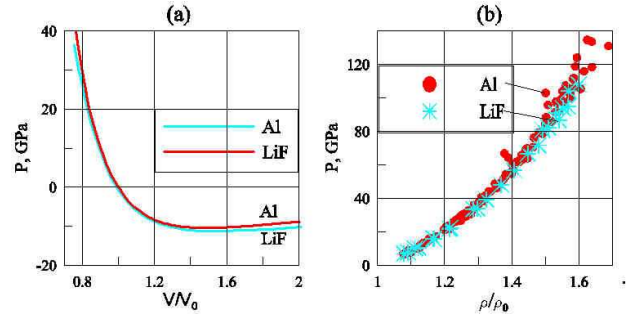


Figure 3. a) Cold pressure curves ($T=0$ isotherms) and b) shock adiabat curves for LiF and Al.

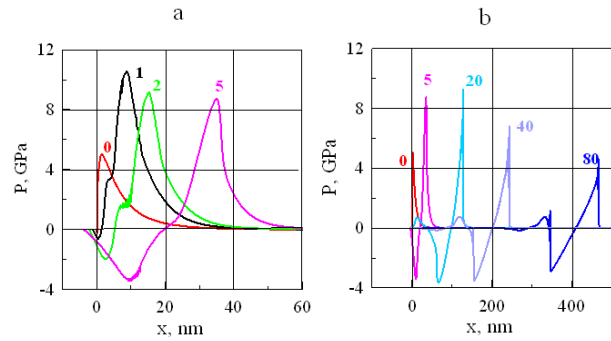


Figure 4. a) Formation of compression wave after action of EUV-FEL pulse in the ablation near-threshold regime with $\tau_L=300$ fs and fluence $F=10$ mJ/cm². The square marker in the pressure profile for the instant $t=5$ ps gives position and absolute value of the maximum instant negative pressure at this instant. b) Appearance of a shock wave as a result of breaking of compression wave, $\tau_L=300$ fs, $F=10$ mJ/cm². Two shocks appear: one before the compression wave, while other behind the stretching wave. There is also appearance of a second compression and second stretching behind main “plus and minus” acoustic pulse. Numbers at lines—time, ps (a and b).

of LiF. Of kinetic coefficients in our equations ν_{imp} is the frequency of the impact ionization and κ_r is a coefficient of three body recombination taken from [2]. When calculating the electron-ion coupling factor α , governing the electron-ion energy exchange, we have taken into account a strong interaction of conduction electrons with the longitudinal optical phonons of the ionic crystal and the fact that the ionic crystal tends to be covalent type crystal with increase of concentration of free carriers. At large concentrations an ionic crystal transforms to a configuration similar to a covalent crystal since positive excess of electron charge of F^- ion gradually disappears as number of electrons lifted from valent band increases. This processes leads to a growth of α from its zero initial value with electron temperature increase followed by the succeeding decrease with a maximum, approximately twice greater than the value of α for aluminum.

Equations (1-6) has been used to simulate action of EUV-FEL onto LiF dielectric within the laser parameters corresponding to the experimental conditions ($\tau_L=300$ fs, $\varepsilon_\gamma=20.2$ eV). Formation and propagation of shock after EUV-FEL action are shown in Fig. 4.

Heat penetration depth in LiF is smaller than in the

case of metals[3] since the stage of supersonic propagation of electron heat wave[4] is absent in dielectrics (while a skin-depth in metals for optical lasers is comparable with D_{att}). That is why the shock wave in LiF appears earlier than in metals.

At instant $t = 0$ a half of fluence is delivered. Maximum of a total pressure $p = p_i + p_e$ is achieved slightly later after the end of a heating laser pulse. Because, firstly, two-temperature relaxation lasts longer than $\tau_L = 300$ fs, and, secondly, electronic gas is softer than condensed matter (at equal internal energies of electron and ion subsystems p_e is smaller than p_i). Passing some distance, the compression wave breaks due to its non-linearity and forms a shock wave. The more non-linear is the wave (larger F, p), the faster it breaks. Shock decays during its subsequent propagation into the bulk. Shock attenuation is faster for more non-linear shock. This attenuation is connected with rarefaction wave coming to the shock from the vacuum boundary side.

Near threshold fluence $F_{abl} = 10$ mJ/cm² the maximum electron temperature is $T_i \simeq 20$ kK, the maximum ionization degree is near 3%. Two-temperature relaxation lasts $t_{eq} \simeq 1$ ps. Maximum T_i is 1.5 kK. For fluence $F = 180$ mJ/cm² we have: $T_e^{max} = 110$ kK, $Z_{max} = 0.4-0.5$ (in the dense part of LiF where $\rho \simeq 2.6$ g/cm³ near the end of two-temperature relaxation), $T_i^{max} \simeq 10$ kK. Fluence $F = 180$ mJ/cm² is the highest fluence achieved in our EUV-FEL experiments.

EUV-FEL pulses of low fluence value $F \sim F_{abl}$ and having high fluences $F \sim 180$ mJ/cm² produce different negative pressures profiles which are responsible for spallative ablation at low fluence. The spallative

mechanism of ablation has been proposed for explanation of very low values of ablation threshold in the case of XRL[5]. In work[5] only the near-threshold case for Ag XRL has been considered experimentally and theoretically. Here we study ablation in wide range of fluences. In the near-threshold case, negative pressure is achieved in early stages, at shallow depth $\simeq 10$ nm, and its amplitude $|p_{neg}| \simeq 3.5$ GPa is approximately a half of the compression wave amplitude. At large fluences we observe another situation. Negative pressures appear later, and at significant depths, their maximum amplitude is of the same order as in the near-threshold case. But now this amplitude is a negligible part (less than 0.1 for $F = 180$ mJ/cm² of the maximum compression pressure.

1. Bushman A. V., Kanel' G. I., Ni A. L., Fortov V. E. Intense Dynamic Loading of Condensed matter. Taylor & Francis, 1993.
2. Sobelman I. I., L. A. Vainshtein L. A., Yukov E. A. Excitation of Atoms and Broadening of Spectral Lines. Springer Series on Atoms and Plasma, Springer, 2007.
3. Inogamov N. A., Zhakhovskii V. V., Ashitkov S. I., Khokhlov V. A., Petrov Yu. V., Komarov P. S., Agranat M. B., Anisimov S. I., Nishihara K. //Appl. Surf. Sci. 2009. V. 255. p. 9712.
4. Inogamov N. A., Petrov Yu. V. //JETP 2010. V. 110. p. 446.
5. Inogamov N. A., Faenov A. Yu., Khokhlov V. A., Zhakhovskii V. V., Petrov Yu. V., Skobelev I. Yu., Nishihara K., Kato Y., Tanaka M., Pikuz T., Kishimoto M., Ishino M., Nishikino M., Fukuda Y., Bulanov S. V., Kawachi T., Anisimov S. I., Fortov V. E. // Contrib. Plasma Phys. 2009. V. 49. p. 455.

NANOSECOND FRAME PHOTOGRAPHY OF QUASI-DETONATION IN SILICA-BASED OPTICAL FIBERS UNDER LASER RADIATION

*Efremov V.P.*¹, Dianov E.M.², Fortov V.E.¹, Bufetov L.A.², Frolov A.A.²*

¹JIHT RAS, ²FORC RAS, Moscow, Russia

*efremov@ihed.ras.ru

Abstract. Destruction wave propagating with high velocities (~ 3 km/s) through the core of silica-based fiber under intensive laser radiation has been investigated. Such regimes were detected at all investigated core diameters of silica-based fibers ($D_C \sim 1.5 - 10 \mu\text{m}$). Plasma and destruction waves in optical fiber were recorded at laser beam intensity up to ~ 40 W/ μm^2 with camera exposition time 2 ns for the first time. Dense plasma propagation takes place together with movement of cracks zone at investigated energy densities in core. Measurements of temperatures for both “start-stop” points and process of propagating were carried out. The measured radiating temperature for “start-stop” points was ~ 11 kK and for detonation-like regime “observed” temperature was ~ 9.4 kK.

Introduction. Laser-induced core damage remains a limiting factor of laser energy transport by optical fiber.

Laser driven detonation (fast) and combustion (slow) waves in air were observed in 1964 [1, 2] and 1969 [3], respectively. The continuous transition be-

tween these regimes (also in air) was observed in [4]. Silica-based optical fibers gave new possibility for investigation of laser-driven destruction waves in solids. Such fibers enabled one to observe the light combustion (also known as fiber fuse effect [5, 6]) and laser-driven detonation-like processes [7] along lengthy tracks. Critical laser radiation intensity for fast regime for gas (air at normal conditions [4]) was found to be ~ 0.05 W/ μm^2 and for fiber glass core ~ 20 W/ μm^2 [7]. Average deposited specific energy was ~ 20 kJ/g for gas and ~ 4.5 kJ/g for fiber core. Propagation velocities of plasma and destruction zone up to ~ 3 km/s were obtained and measured (for laser radiation intensity of ~ 40 W/ μm^2 in the fiber core) [7].

Experiments. In the present work we have continued investigation of detonation-like regimes. These regimes were obtained at all investigated diameters of fiber core 1.5–10 μm (See Fig. 1). One can see increase of crushability of surrounding silica cladding with increasing core diameter. Maximal level of destruction is observed in the vicinity of discharge stop zone. Driving laser pulse was the same as in our previous work [7].